



Monitoring the Subsidence Induced by Salt Mining in Tuzla, Bosnia and Herzegovina by SBAS-DInSAR Method

I. N. S. Parwata¹ · N. Shimizu¹ · B. Grujić² · S. Zekan³ · R. Čeliković³ · E. Imamović⁴ · I. Vrkljan⁵

Received: 24 September 2019 / Accepted: 22 July 2020 / Published online: 1 August 2020
© Springer-Verlag GmbH Austria, part of Springer Nature 2020

Abstract

The ground subsidence induced by salt mining has been causing significant damage in Tuzla, Bosnia and Herzegovina since the 1950s. Several investigations and geodetic surveys have been conducted, i.e., traditional topographic surveys (1950–2003) and static GPS surveys (2004–2007). The last GPS survey (2006–2007) revealed that the subsidence in Tuzla was still occurring at a rate of about – 10 cm/year in some areas. Although monitoring of the subsidence has been on-going at a few points since 2010, by means of the real-time kinematic GNSS method, it lacks spatial coverage. Therefore, an appropriate method is required to monitor the subsidence over an extensive area at a low cost and with less labor time. Differential Interferometry Synthetic Aperture Radar (DInSAR), together with the Small Baseline Subset (SBAS) time-series algorithm, is one of the solutions for use as an effective monitoring tool. The spatial distribution of the subsidence obtained by SBAS-DInSAR shows a good agreement with the subsidence obtained from the former monitoring results. The temporal transition of the subsidence obtained by SBAS-DInSAR is evaluated using the results by the real-time kinematic GNSS monitoring system. It was shown that the DInSAR results coincide with the GNSS results with a discrepancy of less than 10 mm. SBAS-DInSAR detected that the subsidence had almost vanished everywhere, except the north and northeast portions of Pannonica Lake where the rate of subsidence was – 1 to – 4 cm/year during the period of October 2014–May 2019. This study demonstrates that SBAS-DInSAR can be employed as a useful and effective subsidence monitoring tool without the need to install any devices in the monitoring area.

Keywords Subsidence monitoring · Salt mining · SBAS-DInSAR · GNSS/GPS

Abbreviations

AW3D30 ALOS World 3D—30-m resolution digital elevation model
DEM Digital Elevation Model

DInSAR Differential Interferometry Synthetic Aperture Radar
GIS Geographic Information System
GNSS Global Navigation Satellite System
GPS Global Positioning System
InSAR Interferometry Synthetic Aperture Radar
JAXA Japan Aerospace Exploration Agency
LOS Line of Sight
SAR Synthetic Aperture Radar
SBAS Small Baseline Subset

✉ I. N. S. Parwata
sudi_jbc@yahoo.com

- ¹ Graduate School of Science and Engineering, Yamaguchi University, 2-16-1 Tokiwadai, Ube, Yamaguchi Prefecture 755-8611, Japan
- ² Faculty of Architecture, Civil Engineering and Geodesy, University of Banja Luka, Bulevar vojvode Stepe Stepanovića 77/3, 78000 Banja Luka, Bosnia and Herzegovina
- ³ Faculty of Mining, Geology and Civil Engineering, University of Tuzla, Univerzitetska 2, 75000 Tuzla, Bosnia and Herzegovina
- ⁴ Municipality of Tuzla, ZAVNOBiH-a 11, 75000 Tuzla, Bosnia and Herzegovina
- ⁵ Faculty of Civil Engineering, University of Rijeka, Radmile Matejčić 3, 51000 Rijeka, Croatia

List of Symbols

λ Wavelength
 θ_0 Off-nadir angle
 θ_i Incidence angle
 β Angle of the satellite flight (orbit) direction
 D_{sub} Subsidence
 D_{LOS} Displacement along satellite's line of sight (LOS)
 $D_{\text{N-S}}$ Displacement in North–South direction

D_{E-W}	Displacement in East–West direction
D_{U-P}	Displacement in Up–Down (vertical) direction

1 Introduction

The subsidence in Tuzla has been causing significant damage for a long period of time, mainly since 1950. It has been reported that the major factor in this subsidence is the salt mining activities (Mancini et al. 2009a, b; Stecchi 2008; Stecchi et al. 2009). Subsidence of up to -12 m was reported to have been measured by traditional topographic surveys from 1956 to 2003 (Mancini et al. 2009b). The next series of studies on the subsidence in Tuzla was conducted four times by means of static GPS surveys in 2004, 2005, 2006, and 2007 (Mancini et al. 2009a; Stecchi 2008). These GPS surveys produced subsidence information for three periods, namely, 2004–2005, 2005–2006, and 2006–2007, and it was found that the subsidence was generally decreasing, except in the area near Pannonica Lake (Mancini et al. 2009a; Stecchi 2008).

The present subsidence is being monitored by means of classical geodetic measurement and the real-time kinematic GNSS monitoring system. Three GNSS stations have been installed: one is for the reference point and the other two are for measurement points (Čeliković and Imamović 2016). Although the GNSS/GPS system can provide continuous monitoring results, they are obtained only at monitoring points which have been installed with sensors. Therefore, the results show a lack of spatial coverage.

The problems of subsidence monitoring in Tuzla can be summarized as follows: (1) there is a lack of information on the spatial distribution of the current subsidence, (2) conducting conventional, annual or periodical GPS surveys is costly, requires labor and time, and involves difficulties in terms of obtaining the continuous temporal transition of the subsidence, and (3) the installation of a number of real-time kinematic GNSS sensors is one solution for improving the spatial and temporal coverage of the monitoring results; however, it is costly.

Therefore, an efficient, effective, and economical method is required to overcome the above problems. Differential Interferometric Synthetic Aperture Radar (DInSAR) is employed in this study. With DInSAR, it is possible to measure ground surface displacements with accuracy of a few centimeters from the satellite data which were taken more than 500–700 km away from the Earth's surface (Ferretti 2014). This accuracy can be improved by applying several error corrections and using a large amount of satellite data (Berardino et al. 2002; Ferretti et al. 2000). The other advantages of DInSAR are that it can monitor extensive areas (i.e., over thousands of square kilometers) without any sensors or targets on the ground surface.

DInSAR had been applied to various projects related to rock mechanics and geotechnical engineering, such as land subsidence (Vervoort and Declercq 2018; Wempen and McCarter 2017), landslides (Barla 2018; Piane et al. 2016), and other ground displacements (Ciantia et al. 2018; Janna et al. 2012; Rutqvist et al. 2016). Several examples of the application of DInSAR related to ground movement induced by mining activities have been given by Herrera et al. (2010), Vervoort and Declercq (2018), Wempen and McCarter (2017), and Woo et al. (2012). Those researches demonstrated the applicability and effectiveness of DInSAR; however, the results were seen to depend on the ground surface conditions, topography, and other conditions. Therefore, the availability of its application must be investigated in detail and the computing process should be tuned appropriately for each applied case.

The main purposes of this study are: (1) to evaluate the validity and applicability of DInSAR to monitor the subsidence in the target area from the viewpoints of spatial distribution and temporal transition and (2) to enhance the former subsidence information and to provide the present situation of the subsidence in Tuzla. In this study, the Synthetic Aperture Radar (SAR) data from the Sentinel-1A and -1B satellites, operated by the European Space Agency (ESA), are used. The Small Baseline Subset algorithm (Berardino et al. 2002) is employed to obtain the time-series subsidence.

2 Subsidence in Tuzla

The study area is located in Tuzla City, in the northeast part of Bosnia and Herzegovina. Tuzla is the third largest city in Bosnia and Herzegovina. It has a population of about 110,000. Tuzla is famous for salt mining, and massive salt exploitation was conducted during the years of 1956–1988 (Mancini et al. 2009b).

2.1 Geological Setting and Salt Mining History

The Tuzla salt deposit geology has been investigated by several authors (Cicic 2002; Hrvatovic 2006; Jovanovic 1968, 1980; Katzer 1903; Soklllic 1959, 1964, 1982; Stevanovic 1977; Tari and Pamir 1998; Vrabac 1999). The Tuzla salt deposit is located beneath Tuzla City in an area of approximately 2 km² (Fig. 1a). It consists of five separated salt series, or stratigraphic layers, which contain salt rocks embedded in a syncline with one of the limbs close to the surface of the city's center (Fig. 1b and c). The maximum thickness of the salt formation is about 600 m. It is composed of marls and clayey sandstones, salt rocks, banded marls, and anhydrite rocks, as shown by the vertical cross section of $X-X'$ in Fig. 1c.

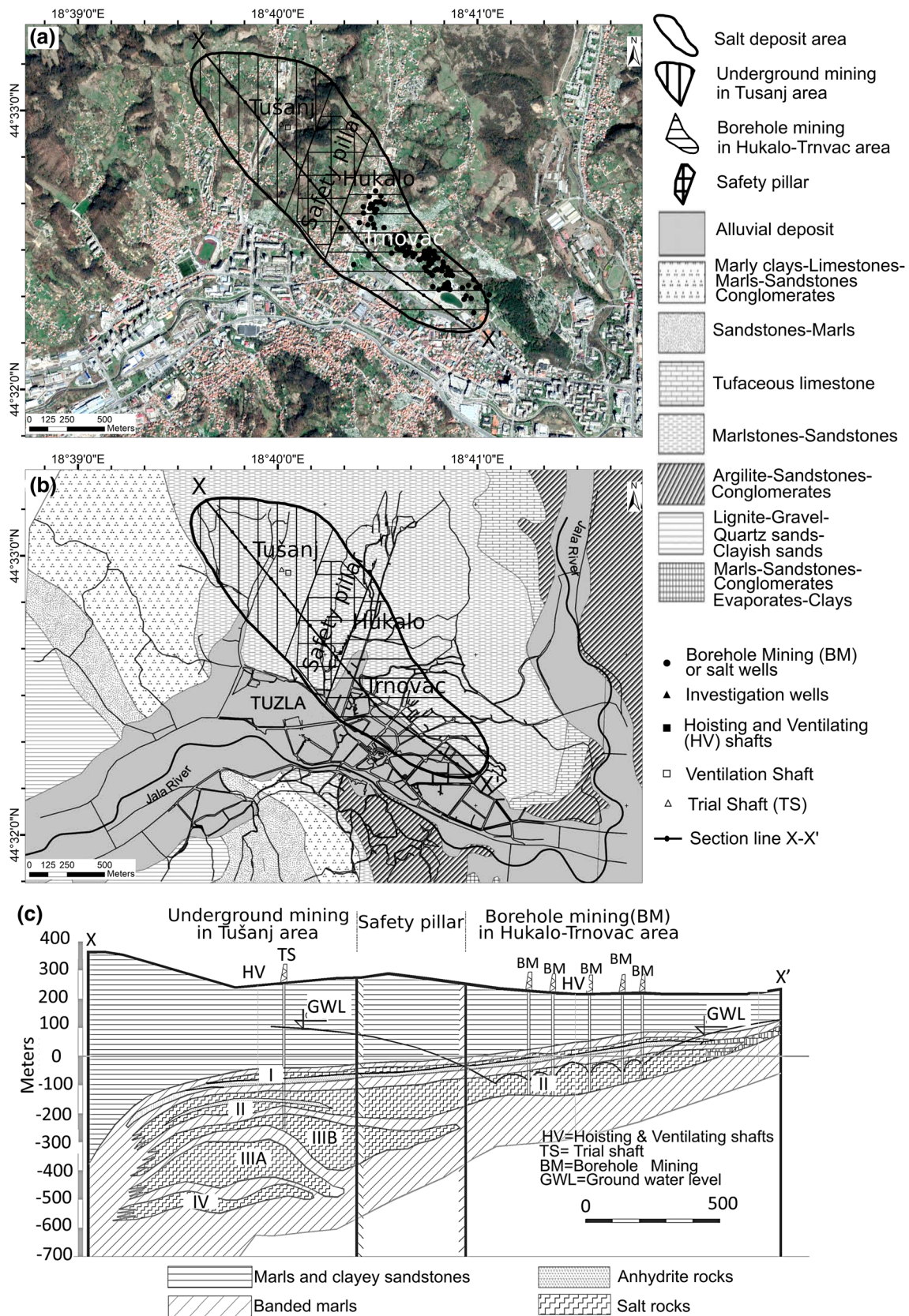


Fig. 1 Geological conditions of Tuzla: **a** plan view using background aerial photo from Google Earth Pro and location of salt wells, **b** plan view (modified from Mancini et al. 2009a), and **c** vertical X-X' cross section (Ferhatbegović 2004)

The origin of the salt deposit is related to the geology of the Pannonian Basin and the Paratethys Sea. The Paratethys was a large shelf sea, stretching from Germany to China, during the beginning of the Oligocene epoch (about 34 million years ago). After paleogeographic changes, the Black Sea, Caspian Lake, and Aral Lake are today's remnants of the Paratethys Sea. The Tuzla Basin was one of the most important basins at the southern edge of the Central Paratethys (Pannonian Basin) during the Miocene epoch (from the Badenian stage to the Pontian stage). The conditions of the lagoon sedimentation and the arid climate contributed to the formation of salt deposits in the Tuzla region during the Early Badenian stage. For a relatively short geological period, the Central Paratethys was isolated, but for most of the time, it was connected to the Eastern Paratethys (Vrabac 2005). The rock salt deposit is located inside the banded marls. It consists of five series, marked as I, II, IIIA, IIIB, and IV in Fig. 1c (Ferhatbegović 2004).

The primitive salt exploitation was done by natural brine and shallow salt water wells in the Neolithic period 6000 years ago. This was confirmed by the discovery of ceramic fragments of holders from 3500 BC, used to boil salt water above hot charcoal (Bakalovic 2005; Stecchi 2008). During the Ottoman-Turkish Empire, salt water exploitation was done by shallow wells, at depths of about 60 m, and the production of salt in that period amounted to 2500 kg/day (Jokanović 1952).

Industrial exploitation of the salt deposit in Tuzla had been developed in two separated mining fields, i.e., underground salt mining in Tušanj and borehole salt mining (extraction of salt water) in Hukalo–Trnovac. The deposit between the two mining fields was not mined so as to leave it as a safety pillar, as shown in Fig. 1 (Ferhatbegović 2004).

Underground mining was conducted in Tušanj from 1967 to 2002 by means of the classical room-pillar method and the extraction of crude dry salt. Also, in the same field, the so-called “controlled leaching” was conducted in lower mining rooms to extract dissolved salt, which was pumped out of the underground mine through pipelines. The Tušanj mine was flooded by dissolved salt and had to be closed from 2002 to 2004 (Tomić et al. 2005). Salt water extraction was conducted in Hukalo–Trnovac from 1906 to 2006 using a borehole method (Čeliković et al. 2014). This method is known as the “uncontrolled leaching method” because it is impossible to control which part of the deposit is leached. The location of boreholes (salt wells) is indicated by bullets in Fig. 1a. Borehole salt mining was initially carried out by the injection of fresh water to speed up the dissolution process. The fresh water injection process was conducted for only six months; it was stopped due to the appearance of a 50-m-diameter sinkhole in a suburban area in 1987 (Mancini et al. 2009a; Stecchi et al. 2009). The area between the underground mining in Tušanj and the borehole mining in

Hukalo–Trnovac was unexcavated and left as a safety pillar. A safety pillar is a type of natural protection; it does not require any additional construction work or reinforcements (Ferhatbegović 2004).

The intensive production of salt water (by the uncontrolled leaching method) caused extensive subsidence of up to -12 m in the urban area of Tuzla. It induced serious damage to buildings and the infrastructure, such as water supply systems, sewage networks, and electric powerlines (Stecchi et al. 2009). For this reason, more than 2000 buildings collapsed or needed to be demolished and about 15,000 people had to evacuate the most affected area (Stecchi et al. 2009). Another report (Ibreljic et al. 2007) mentioned that 2300 apartments were ruined between 1965 and 1990 due to the subsidence phenomenon. The decision to stop the exploitation of salt was made to reduce the subsidence. In the period from March 2006 to May 2007, a gradual suspension of the salt well exploitation was carried out. The official date of termination of the Tuzla salt deposit exploitation is May 29, 2007 (Čeliković and Imamović 2016).

2.2 Former Monitoring Results of Subsidence

Several investigations and geodetic surveys have been conducted to monitor the subsidence in different periods, i.e., traditional topographic surveys (1950–2003) (Mancini et al. 2009b), static GPS surveys (2004–2007) (Stecchi 2008), and real-time kinematic GNSS monitoring (2010–present day) (Čeliković and Imamović 2016).

2.2.1 Traditional Topographic Surveys Until 2003

The first geodetic survey was conducted in Tuzla in 1914 (Mancini 2009b). However, a systematic survey to measure the subsidence due to salt mining was not started until 1956. It was continued until 1992 and ended due to the Balkan War. These long-term surveys produced a large amount of topographical data. The results of the geodetic surveys from 1992–2003 were not as reliable as those from the previous period. One analysis of the topographical data was conducted by Mancini et al. (2009a, b) and revealed that the ground surface had sunk up to -12 m. These results are presented in Fig. 2a by contour lines (Mancini et al. 2009a). It was found that the large subsidence extended to the north part of the city, including the residential area, and was shaped like a bowl.

Figure 2b presents the relationship between the annual average subsidence in cm/year (as a solid line) and the annual amount of brine water pumped in m³ (as a dashed line). The annual volume of extracted salt water was estimated from the mining database, and the annual average subsidence was calculated by the representative subsidence for the whole area and during 1956–1992 (Mancini

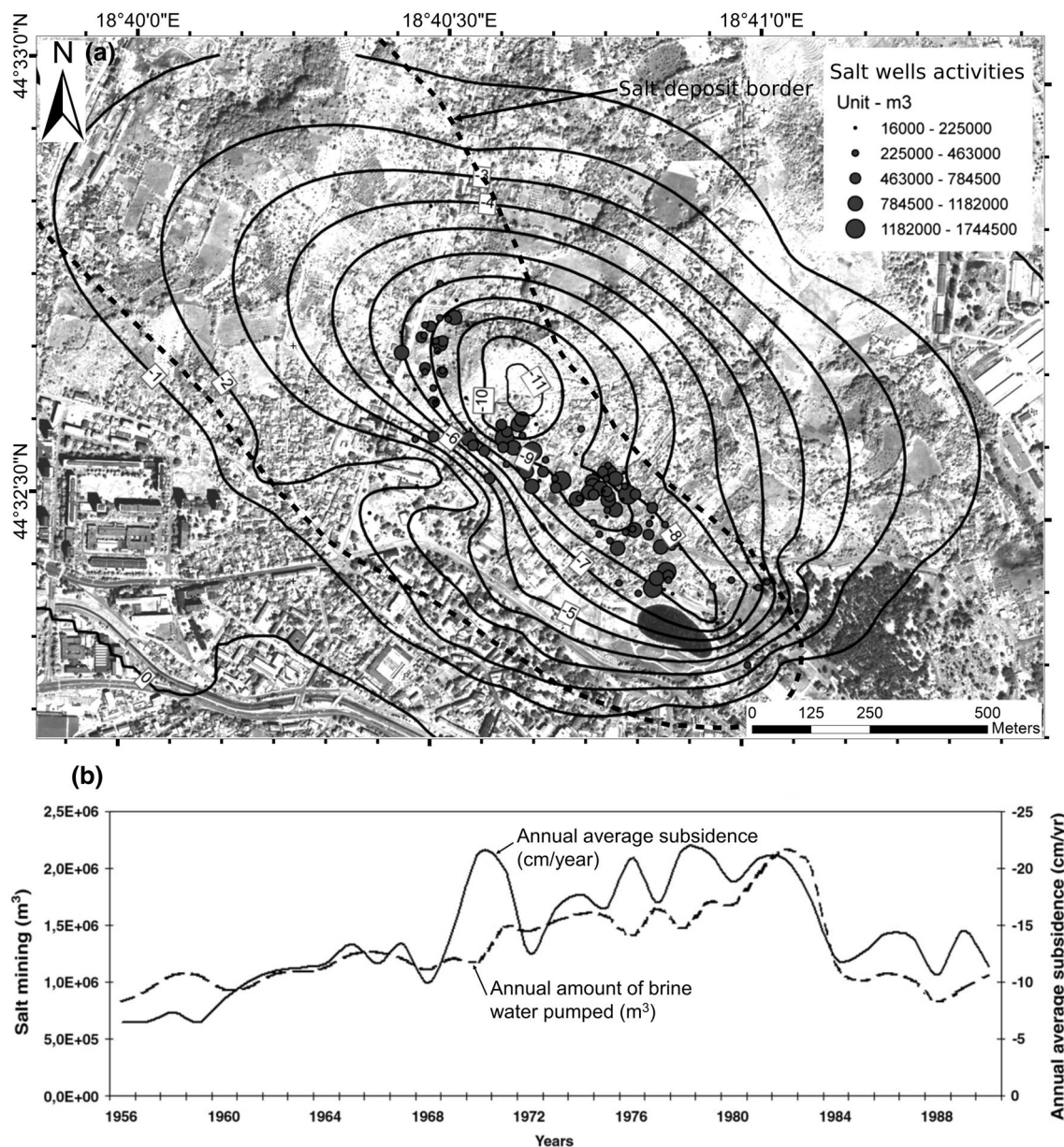


Fig. 2 Cumulative subsidence and its relationship to annual amount of brine water pumped: **a** cumulative subsidence obtained by traditional topographic surveys from 1956 to 2003 presented by contour lines (dashed line indicates salt deposit border added by the authors)

and **b** comparison between annual average subsidence in cm/year (as a solid line) and annual amount of brine water pumped in m³ (as a dashed line). It is limited to the period of 1956–1992 (modified from Mancini et al. 2009a)

et al. 2009a). A remarkable correlation is shown around 1982 when the salt water extractions were reduced and the subsidence rate decreased (Fig. 2b). It is seen that halving the salt water extraction from the year 1982 induced a reduction in the annual subsidence rate to approximately one half of that of the previous value (Mancini et al. 2009a).

2.2.2 Static GPS Surveys

Static GPS surveys were conducted four times, namely, in 2004, 2005, 2006, and 2007 (Mancini et al. 2009a; Stecchi 2008). The survey network was composed of six reference points and 60 densification measurement points (Mancini et al. 2009a). The results of the GPS surveys are presented in

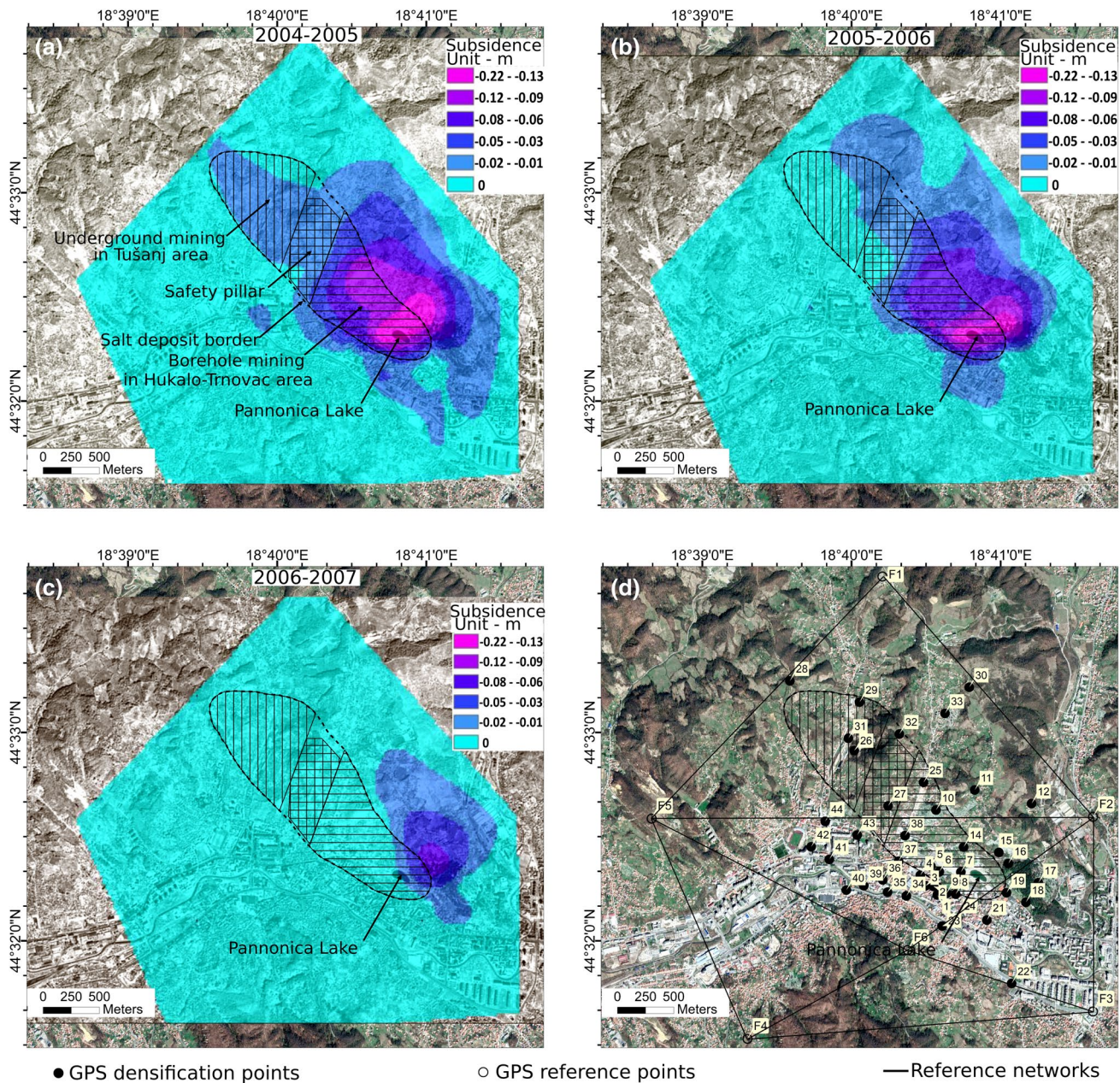


Fig. 3 Subsidence in Tuzla obtained by GPS surveys: **a** subsidence from 2004 to 2005, **b** subsidence from 2005 to 2006, **c** subsidence from 2006 to 2007 (modified from Stecchi (2008) (salt deposit bor-

der, safety pillar, and mining region were added by the authors), and **d** map of GPS densification and reference points (re-drawn from Stecchi (2008) and Mancini et al. (2009a))

Fig. 3. Figure 3a–c shows the subsidence distributions, while Fig. 3d shows the location of the densification and reference points of the GPS surveys.

The GPS results for 2004–2005 show that the subsidence continued at a rate of -12 to -22 cm/year in the north part of Pannonica Lake (Fig. 3a), although the subsidence rate had decreased a great deal compared with that of the previous period (1956–2003). A considerable part of the northeast portion of the city was subjected

to subsidence rates of -2 to -5 cm/year. In the period of 2005–2006, the subsidence rate decreased to -8 to -22 cm/year around Pannonica Lake (Fig. 3b). Mancini et al. (2009a) and Stecchi (2008) stated that the last GPS results from 2006 to 2007 showed that the subsidence was heading to the end almost everywhere, except for the area near Pannonica Lake where the subsidence rate was still about 10 cm/year (Mancini et al. 2009a; Stecchi 2008).

2.2.3 Real-time Kinematic GNSS Monitoring

The real-time kinematic GNSS monitoring system has been installed for monitoring the subsidence in Tuzla. Three GNSS sensors were installed in the city (Čeliković and Imamović 2016). The results will be shown in Sect. 4.2.

3 Procedure of Multi-temporal DInSAR

3.1 Outline of SBAS-DInSAR

SAR is an active remote sensing device which can be used day and night to produce high resolution images (3–15 m of spatial resolution on the Earth's surface). It is mounted on a satellite, and transmits microwave signals in a side-looking direction (Fig. 4) with specific wavelength λ (band) to the Earth's surface and receives its reflected waves. There are several types of SAR bands, e.g., X-band ($\lambda = 2.5\text{--}3.75$ cm), C-band ($\lambda = 3.75\text{--}7.5$ cm), and L-band ($\lambda = 15\text{--}30$ cm). The amplitude and phase of the reflected waves are observed and stored in one file referred to as the SAR data.

DInSAR is a method for observing the displacements of the Earth's surface using the SAR data (Ferretti 2007). It can detect changes in the distance between the satellite and the Earth's surface by utilizing two sets of SAR data taken in

the same area on the Earth's surface, but at different times and at slightly different satellite positions. These changes in distance can be interpreted as the displacements of the Earth's surface in the direction of the line along which the waves are transmitted. This direction is called the line of sight (LOS) (Fig. 4). The LOS displacements are similar in quantity to the displacements measured by an extensometer.

The time difference between the first and second periods of data acquisition is called the temporal baseline length, and the distance between the two satellite positions is called the spatial baseline length. DInSAR does not directly measure the displacements of the ground surface, but it calculates the phase difference of the two sets of SAR data. The spatial distribution of the phase difference is called an interferogram. It includes the effects of the satellite baseline length and the topography of the Earth's surface. To obtain the displacement from the interferogram, such effects should be removed using the satellite information and the Digital Elevation Model (DEM). The displacement is determined for each pixel on the Earth's surface. This is the basic process of DInSAR for measuring the displacement distribution on the Earth's surface (Ferretti et al. 2007).

When continuous displacement monitoring is conducted by DInSAR, a time-series analysis is applied to many pairs of SAR data. The SBAS method (Berardino et al. 2002) could be a useful tool for this analysis. SBAS is implemented using the SAR data pairs with small spatial and temporal baseline lengths, selected by giving the threshold of both baseline lengths, in order to reduce the errors caused by long spatial and temporal baseline lengths. After conducting the DInSAR process to obtain the incremental displacement for each pair of SAR data, the mean velocity of the displacement for each period is estimated (Berardino et al. 2002). During this process, the errors due to the residual topography, the atmospheric phase delay, and other random error sources can be reduced (Berardino et al. 2002; Lanari et al. 2007). A simplified flowchart for SBAS is given in Fig. 5. After all the errors have been reduced, the time-series of the displacement can be obtained, and further analysis and an interpretation of the results can be conducted using Geographic Information System (GIS) software.

3.2 Data Collection

The SAR data acquired with TOPSAR (Zan and Guarnieri 2006) by means of the Sentinel-1A and Sentinel-1B satellites, operated by the ESA, are used in this study. Since the data from Sentinel-1A and -1B are free, economical monitoring can be realized.

The total amount of data used in this study are 199 sets of SAR data (Table 1), which were taken from October 9, 2014 to May 28, 2019 in the descending orbit direction. The path and the frame numbers of the SAR data are 51

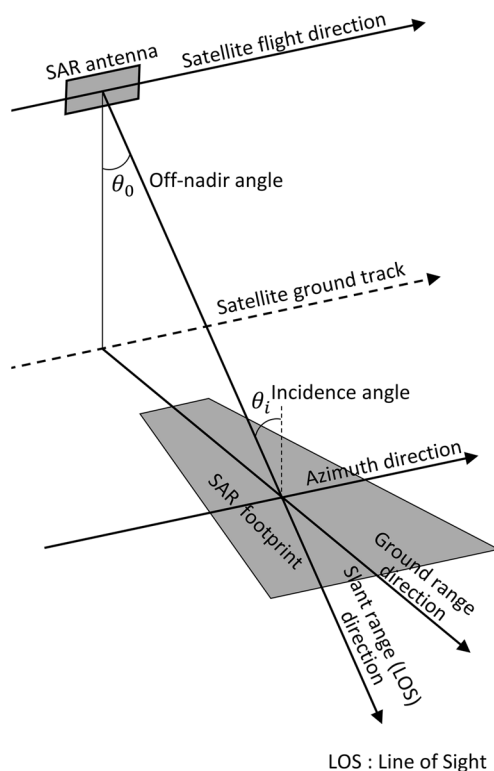


Fig. 4 Geometrical view of SAR system

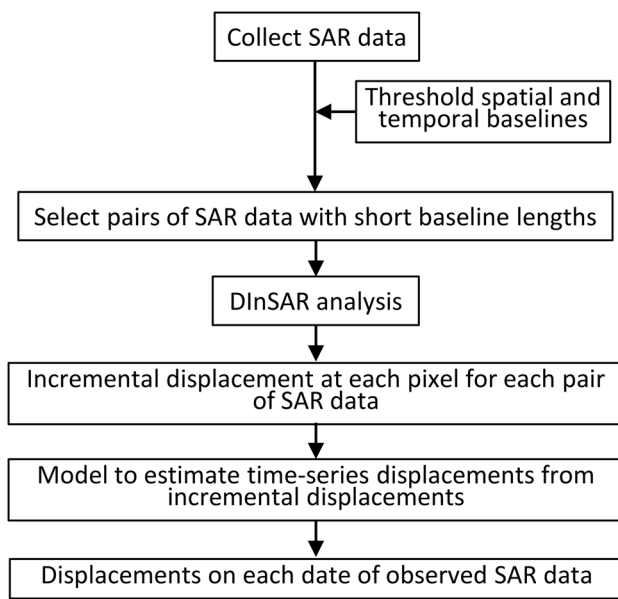


Fig. 5 Flowchart of SBAS (simplified)

and 442–446, respectively. Since Sentinel-1A and -1B are in active operation, the amount of SAR data can be updated every 6–12 days.

3.3 SBAS Processing Steps

In this study, Envi SARscape version 5.5.2 (SARMAP 2019) is used as the SAR processor for conducting the SBAS-DInSAR analysis. The first step is the selection of the SAR data pair combinations by assigning threshold values to the temporal and spatial baselines. The maximum temporal baseline and the maximum spatial baseline are set at 48 days and 150 m, respectively. This produces possible combinations from the 199 sets of SAR data (Table 1), as shown in Fig. 6. These threshold values result in a total of 544 combinations (interferograms) to be analyzed. Then, all possible pairs, presented in Fig. 6, are processed using the conventional DInSAR method. The digital elevation model (DEM) provided by JAXA (Japan Aerospace Exploration Agency), ALOS World 3D—30 m (AW3D30) (Takaku and Tadono 2017), is used to remove the topographic phase effects. The interferograms and the coherence, which is an index representing the reliability of the results of the interferograms, were produced in this step and then checked. The eight sets of SAR data with low coherence (presented by the red diamonds in Fig. 6) are removed from the SBAS analysis to reduce the errors in the analyses.

After the SBAS process, the time-series spatial distribution of the LOS displacements is obtained for all the dates on which the SAR data were observed. The spatial resolution of the displacement is 25 m × 25 m in this study.

3.4 Derivation of Subsidence from Measured LOS Displacements

The displacements obtained by SBAS-DInSAR are in one dimension along the line of sight (LOS), as mentioned in Sect. 3.1. To convert the LOS displacements to subsidence, a simple assumption is employed, namely, as the displacements are mainly caused by subsidence (vertical movements), the horizontal displacements can be ignored. Under such an assumption, the relationship between LOS displacement D_{LOS} and subsidence D_{Sub} is shown in Fig. 7, and the subsidence can then be obtained from the LOS displacements by Eq. (1).

$$D_{\text{Sub}} = -\frac{D_{\text{LOS}}}{\cos \theta_i}, \quad (1)$$

where θ_i is the local incidence angle and the subsidence is assigned with a minus sign.

It should be noted that if a non-negligible horizontal displacement arises in the actual behavior, Eq. (1) will include some errors.

4 Results and Validation

4.1 Spatial Distribution

The results of the distribution map of the subsidence were obtained by SBAS-DInSAR, as described in Sect. 3.3. The total number of maps is 198. Figure 8 shows some of them as examples; they indicate the time transition of the subsidence distribution.

It is clearly found that the subsidence increases as time passes in the area north of Pannonica Lake and in the east part of Tušanj. The larger subsidence occurring in the area northeast of Pannonica Lake is represented by orange and red (Fig. 8f). The accumulated subsidence from October 2014 to May 2019 is 100–200 mm in the area northeast of Pannonica Lake, 50–100 mm in the area northwest of Pannonica Lake and the east part of Tušanj (yellow color in Fig. 8f), and less than 50 mm in other areas. Around the safety pillar, which is an unexcavated area, as well as the area outside of the salt deposit around the city area, almost no subsidence has occurred over the last four and a half years.

On the other hand, there are no results for some parts of the map especially in the area with vegetation coverage. This is due to the weak or the lack of microwave reflections and to the changes in the growing situation in high vegetation areas that cause the low coherence of the interferograms, which means SBAS-DInSAR cannot provide reliable measurement

Table 1 List of Sentinel-1A and -1B SAR data used in this study

No.	Date	Satellite	No.	Date	Satellite	No.	Date	Satellite	No.	Date	Satellite
1	2014-10-09	S1A	51	2016-10-22	S1A	101	2017-09-05	S1B	151	2018-08-07	S1B
2	2014-10-21	S1A	52	2016-10-28	S1B	102	2017-09-17	S1B	152	2018-08-19	S1B
3	2014-12-08	S1A	53	2016-11-03	S1A	103	2017-09-29	S1B	153	2018-08-25	S1A
4	2014-12-20	S1A	54	2016-11-09	S1B	104	2017-10-11	S1B	154	2018-08-31	S1B
5	2015-01-01	S1A	55	2016-11-15	S1A	105	2017-10-17	S1A	155	2018-09-06	S1A
6	2015-01-25	S1A	56	2016-11-21	S1B	106	2017-10-23	S1B	156	2018-09-12	S1B
7	2015-02-06	S1A	57	2016-11-27	S1A	107	2017-11-04	S1B	157	2018-09-18	S1A
8	2015-02-18	S1A	58	2016-12-03	S1B	108	2017-11-10	S1A	158	2018-09-24	S1B
9	2015-03-02	S1A	59	2016-12-09	S1A	109	2017-11-16	S1B	159	2018-09-30	S1A
10	2015-03-14	S1A	60	2016-12-15	S1B	110	2017-11-22	S1A	160	2018-10-06	S1B
11	2015-03-26	S1A	61	2016-12-21	S1A	111	2017-11-28	S1B	161	2018-10-12	S1A
12	2015-04-07	S1A	62	2016-12-27	S1B	112	2017-12-10	S1B	162	2018-10-18	S1B
13	2015-05-01	S1A	63	2017-01-02	S1A	113	2017-12-16	S1A	163	2018-10-24	S1A
14	2015-05-13	S1A	64	2017-01-08	S1B	114	2017-12-22	S1B	164	2018-10-30	S1B
15	2015-05-25	S1A	65	2017-01-14	S1A	115	2017-12-28	S1A	165	2018-11-05	S1A
16	2015-06-06	S1A	66	2017-01-20	S1B	116	2018-01-03	S1B	166	2018-11-11	S1B
17	2015-06-18	S1A	67	2017-01-26	S1A	117	2018-01-09	S1A	167	2018-11-17	S1A
18	2015-06-30	S1A	68	2017-02-01	S1B	118	2018-01-15	S1B	168	2018-11-23	S1B
19	2015-07-12	S1A	69	2017-02-07	S1A	119	2018-01-21	S1A	169	2018-11-29	S1A
20	2015-07-24	S1A	70	2017-02-13	S1B	120	2018-01-27	S1B	170	2018-12-05	S1B
21	2015-08-17	S1A	71	2017-02-19	S1A	121	2018-02-02	S1A	171	2018-12-11	S1A
22	2015-08-29	S1A	72	2017-02-25	S1B	122	2018-02-08	S1B	172	2018-12-17	S1B
23	2015-09-10	S1A	73	2017-03-03	S1A	123	2018-02-14	S1A	173	2018-12-23	S1A
24	2015-10-04	S1A	74	2017-03-09	S1B	124	2018-02-20	S1B	174	2018-12-29	S1B
25	2015-10-16	S1A	75	2017-03-15	S1A	125	2018-02-26	S1A	175	2019-01-04	S1A
26	2015-10-28	S1A	76	2017-03-21	S1B	126	2018-03-04	S1B	176	2019-01-10	S1B
27	2015-11-09	S1A	77	2017-03-27	S1A	127	2018-03-10	S1A	177	2019-01-16	S1A
28	2015-11-21	S1A	78	2017-04-02	S1B	128	2018-03-16	S1B	178	2019-01-22	S1B
29	2015-12-03	S1A	79	2017-04-08	S1A	129	2018-03-22	S1A	179	2019-01-28	S1A
30	2015-12-15	S1A	80	2017-04-20	S1A	130	2018-03-28	S1B	180	2019-02-03	S1B
31	2016-01-08	S1A	81	2017-04-26	S1B	131	2018-04-03	S1A	181	2019-02-09	S1A
32	2016-01-20	S1A	82	2017-05-02	S1A	132	2018-04-09	S1B	182	2019-02-15	S1B
33	2016-02-01	S1A	83	2017-05-08	S1B	133	2018-04-15	S1A	183	2019-02-21	S1A
34	2016-02-25	S1A	84	2017-05-14	S1A	134	2018-04-21	S1B	184	2019-02-27	S1B
35	2016-03-20	S1A	85	2017-05-20	S1B	135	2018-04-27	S1A	185	2019-03-05	S1A
36	2016-04-13	S1A	86	2017-05-26	S1A	136	2018-05-03	S1B	186	2019-03-11	S1B
37	2016-04-25	S1A	87	2017-06-01	S1B	137	2018-05-09	S1A	187	2019-03-17	S1A
38	2016-05-19	S1A	88	2017-06-07	S1A	138	2018-05-15	S1B	188	2019-03-23	S1B
39	2016-05-31	S1A	89	2017-06-13	S1B	139	2018-05-21	S1A	189	2019-03-29	S1A
40	2016-06-12	S1A	90	2017-06-19	S1A	140	2018-05-27	S1B	190	2019-04-04	S1B
41	2016-07-06	S1A	91	2017-06-25	S1B	141	2018-06-08	S1B	191	2019-04-10	S1A
42	2016-07-18	S1A	92	2017-07-01	S1A	142	2018-06-14	S1A	192	2019-04-16	S1B
43	2016-08-11	S1A	93	2017-07-13	S1A	143	2018-06-20	S1B	193	2019-04-22	S1A
44	2016-08-23	S1A	94	2017-07-19	S1B	144	2018-06-26	S1A	194	2019-04-28	S1B
45	2016-09-04	S1A	95	2017-07-25	S1A	145	2018-07-02	S1B	195	2019-05-04	S1A
46	2016-09-16	S1A	96	2017-07-31	S1B	146	2018-07-08	S1A	196	2019-05-10	S1B
47	2016-09-28	S1A	97	2017-08-06	S1A	147	2018-07-14	S1B	197	2019-05-16	S1A
48	2016-10-04	S1B	98	2017-08-12	S1B	148	2018-07-20	S1A	198	2019-05-22	S1B
49	2016-10-10	S1A	99	2017-08-24	S1B	149	2018-07-26	S1B	199	2019-05-28	S1A

Table 1 (continued)

No.	Date	Satellite	No.	Date	Satellite	No.	Date	Satellite	No.	Date	Satellite
50	2016–10–16	S1B	100	2017–08–30	S1A	150	2018–08–01	S1A			

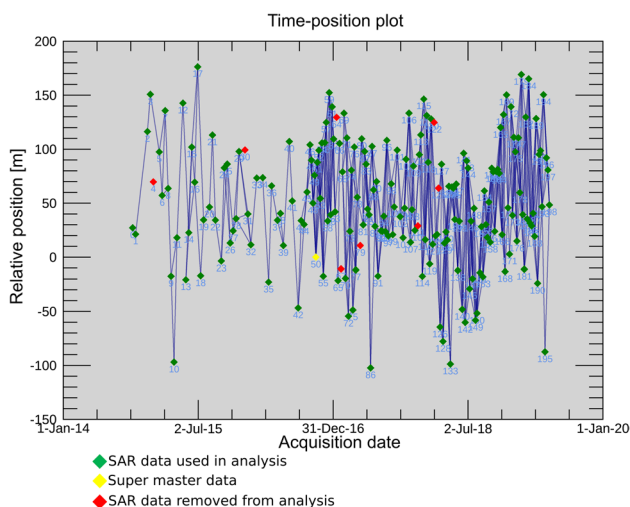


Fig. 6 Combination of SAR pairs used in SBAS-DInSAR analysis. The green diamonds indicate the number of SAR data used in the SBAS-DInSAR analysis, the red diamonds indicate that the SAR data were not used or removed from the SBAS-DInSAR analysis, and the yellow diamond is the super master data

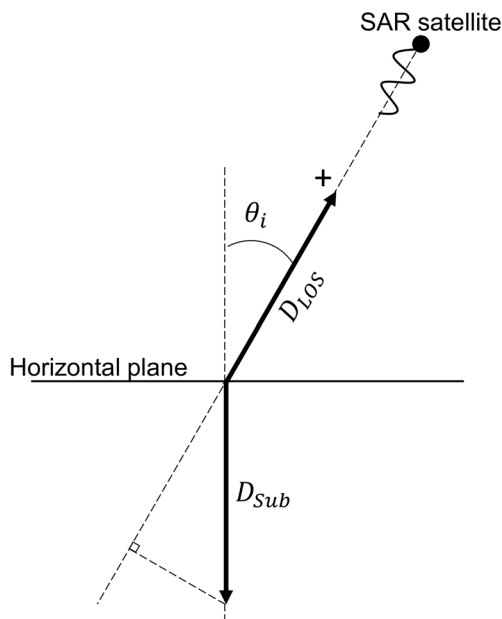


Fig. 7 Relationship between LOS displacements and subsidence under assumption of no horizontal displacement

results (Ferretti 2014). In this research, 0.3 is given as the threshold value of the coherence for interferometry to obtain the results, i.e., the results are not shown for areas where the coherence is less than 0.3.

The spatial distribution of the subsidence obtained by SBAS-DInSAR for a year (from May 2018 to May 2019) is compared with distributions by GPS surveys (from 2006 to 2007) and traditional topographical surveys (from 1956 to 2003) in Fig. 9. It is found that the subsidence distribution by SBAS-DInSAR (Fig. 9a) is different from those by the traditional topographical surveys (Fig. 9c), i.e., the amount of subsidence is much smaller than before and the location of the large subsidence area is seen to have moved from the center of the salt mine region (see Fig. 9c) to the area northeast of Pannonica Lake (see Fig. 9a). This is because, as seen in Fig. 2b, the extraction of salt water was very active in those days (1956–2003).

On the other hand, the subsidence distribution by SBAS-DInSAR is similar to those by the GPS surveys (Fig. 9b). This means that the subsidence has continued in the same place since the last GPS survey even after the termination of the salt water extraction in 2007. As will be seen in Sect. 5.2, the rate of subsidence has decreased since 2007 in almost all areas. The details will be discussed in Sect. 5.2.

4.2 Temporal Transition

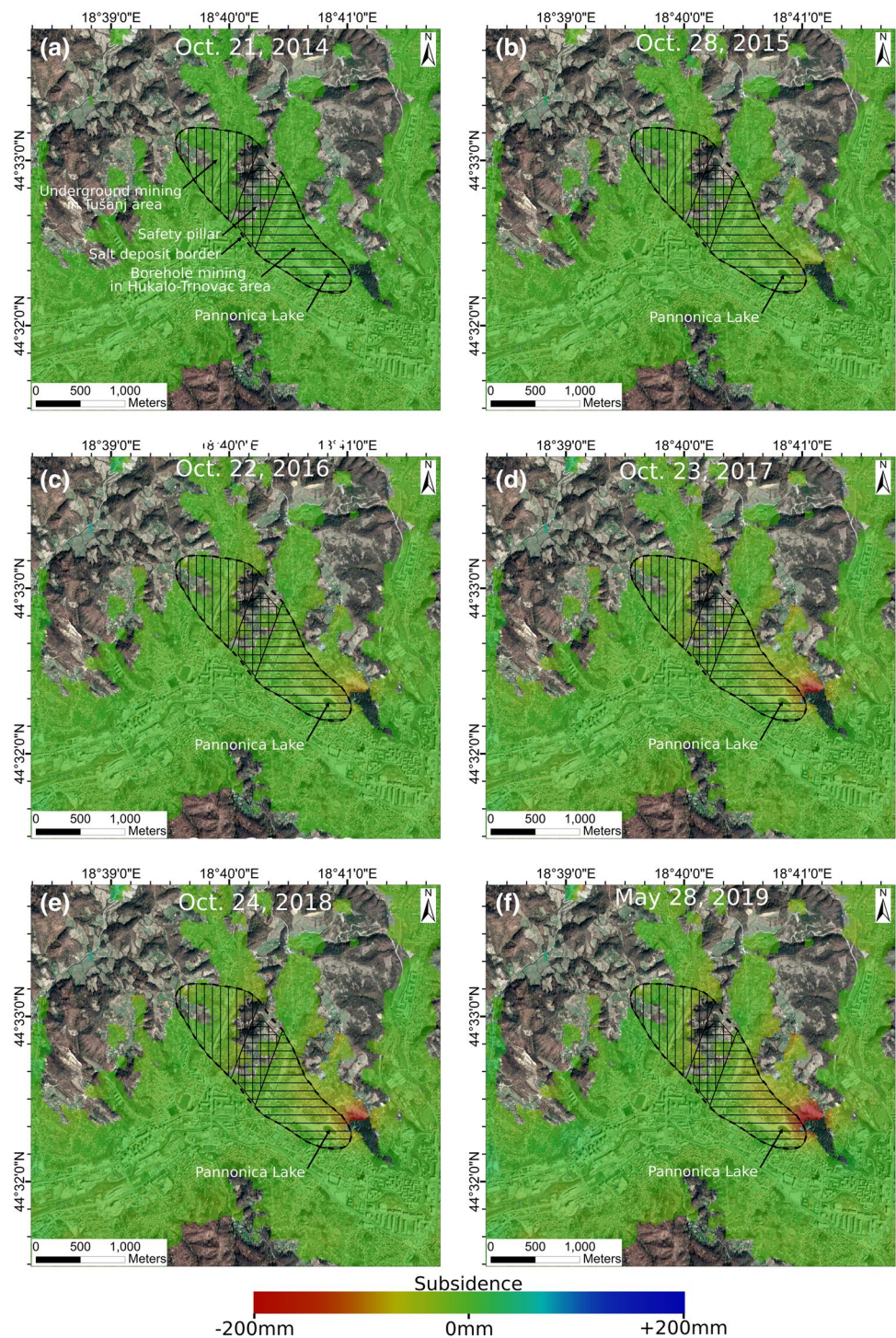
To validate the subsidence transition in time obtained by SBAS-DInSAR, the monitoring results by GNSS are used. GNSS stations have been installed at three points, namely, Tušanj, Pannonica, and Tuzla, and displacements are being monitored at those stations by the real-time kinematic method (Čeliković and Imamović 2016). Tušanj and Pannonica stations are the monitoring points and Tuzla station is the reference (fixed) point.

To make an appropriate comparison, the three-dimensional displacements obtained by GNSS are projected into LOS displacements using the following equation:

$$D_{LOS} = [D_{N-S} \ D_{E-W} \ D_{U-D}] \begin{bmatrix} -\sin \theta_i \cdot \sin \beta \\ \sin \theta_i \cdot \cos \beta \\ \cos \theta_i \end{bmatrix}, \tag{2}$$

where θ_i is the incidence angle of the microwaves transmitted from the satellite and β is the angle of the satellite flight (orbit) direction, as shown in Fig. 10.

Fig. 8 Subsidence distribution obtained by SBAS-DInSAR on several dates: **a** October 21, 2014, **b** October 28, 2015, **c** October 22, 2016, **d** October 23, 2017, **e** October 24, 2018, and **f** May 28, 2019



Comparisons of the LOS displacements by GNSS and SBAS-DInSAR at Tušanj and Pannonica stations are shown in Fig. 11. Since the GNSS results were greatly scattered, very few results could be utilized. The displacements show a good agreement. Figure 12 illustrates the relationship between the SBAS-DInSAR results and the GNSS results at Pannonica and Tušanj stations. It is seen that the SBAS-DInSAR results coincide with the GNSS

results with a discrepancy between them of less than 10 mm. The RMSE (root mean square error) is 4.3 mm for Pannonica station, 1.6 mm for Tušanj station, and 3.9 mm totally for both stations. These results are similar to or better than those reported in other researches (Casu et al. 2006; Hu et al. 2019; Motagh et al. 2017; Qu et al. 2015; Tizzani et al. 2007).

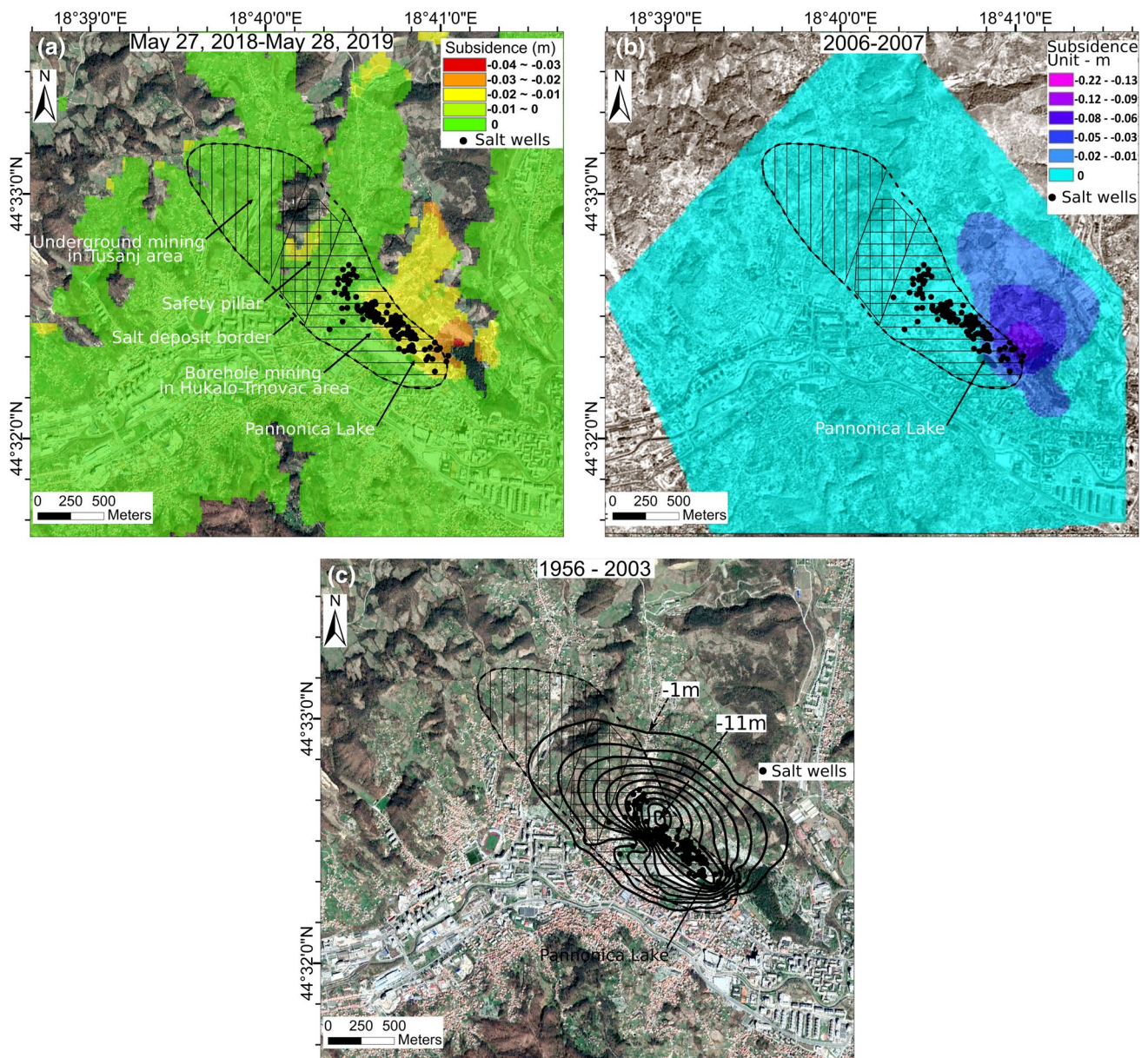


Fig. 9 Comparison of subsidence distributions obtained by different methods and in different periods: **a** subsidence distribution obtained by SBAS-DInSAR from May 27, 2018 to May 28, 2019, **b** subsidence distribution obtained by GPS surveys from 2006–2007 (modified from Stecchi 2008), and **c** subsidence distribution obtained by traditional topographical surveys from 1956 to 2003 (re-drawn from Mancini et al. 2009b)

Figure 11c presents the LOS displacement by SBAS-DInSAR at Tuzla station, which is located far from the subsidence area. The displacement at this station did not increase much over the monitoring period and the accumulated value is less than a few mm. It showed that no remarkable displacement occurred at this point and then Tuzla station was suitable for the reference point of GNSS monitoring.

From the above results, it is found that the SBAS-DInSAR results in this study are acceptable.

from Stecchi 2008), and **c** subsidence distribution obtained by traditional topographical surveys from 1956 to 2003 (re-drawn from Mancini et al. 2009b)

5 Discussions

5.1 Comparison Between Former (1956–2003) and Present (2014–2019) Subsidence in Spatial Distribution

A comparison of the subsidence shapes and values, obtained by the traditional topographical surveys and by SBAS-DInSAR, is illustrated in Fig. 13 in section lines A–A' and B–B'.

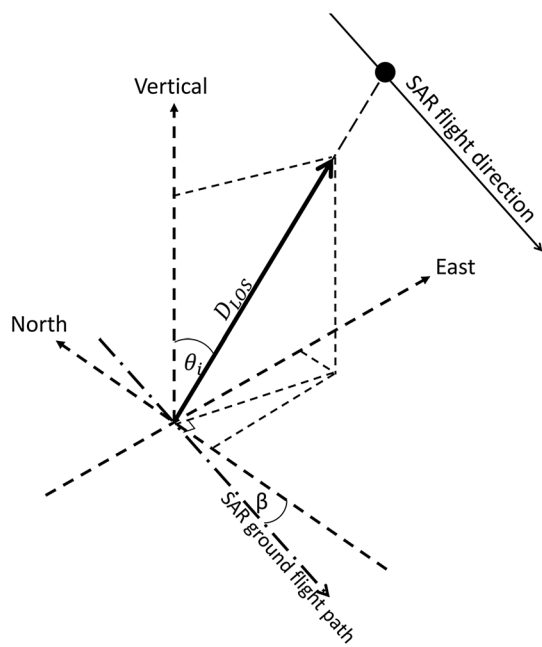


Fig. 10 Geometry of three-dimensional displacements projected into LOS displacements (in descending right-looking orbit direction)

Figure 13c shows the subsidence along section line A–A'. A large subsidence of more than 1 m appeared between 400 and 1400 m on the lateral axis, and its peak (–12 m) was found at a position of around 910 m on the lateral axis during the period of 1956–2003 (Mancini et al. 2009a). According to the SBAS-DInSAR results, the magnitude of subsidence decreased greatly and subsidence of up to –115 mm occurred at a position of 1650 m on the lateral axis during the period of 2014–2019.

The subsidence by SBAS-DInSAR along section line B–B' is shown together with the results of the traditional topographic surveys in Fig. 13d. The figure shows that a subsidence larger than –40 mm occurred between 1000 and 1800 m on the lateral axis during the period of 2014–2019. However, the subsidence along B–B' between 1250 and 1570 m on the lateral axis did not appear because of the low coherence of the interferogram in this portion due to the vegetation conditions.

Section lines A–A' and B–B' were set by Mancini et al. (2009a) to show the shapes and the maximum subsidence obtained by the traditional topographical surveys in the vertical section. In a similar way, to investigate the SBAS-DInSAR results, two section lines, C–C' and D–D', are newly set to present the distributions of subsidence obtained by SBAS-DInSAR, including the maximum subsidence. Figure 13e and f show subsidence of more than –40 mm (up to –160 mm) along lines C–C' and D–D' between about 700 m and 1900 m on the lateral axis, and between about 520 m and 1150 m on the lateral axis, respectively. It is

found that the area of the maximum subsidence is located outside the salt deposit around the northeast portion of Pannonica Lake. The extent of the area of subsidence has been reduced, and the amount of subsidence is much less at the present time.

5.2 Trend of Time Transition of Subsidence from 2004 to 2019

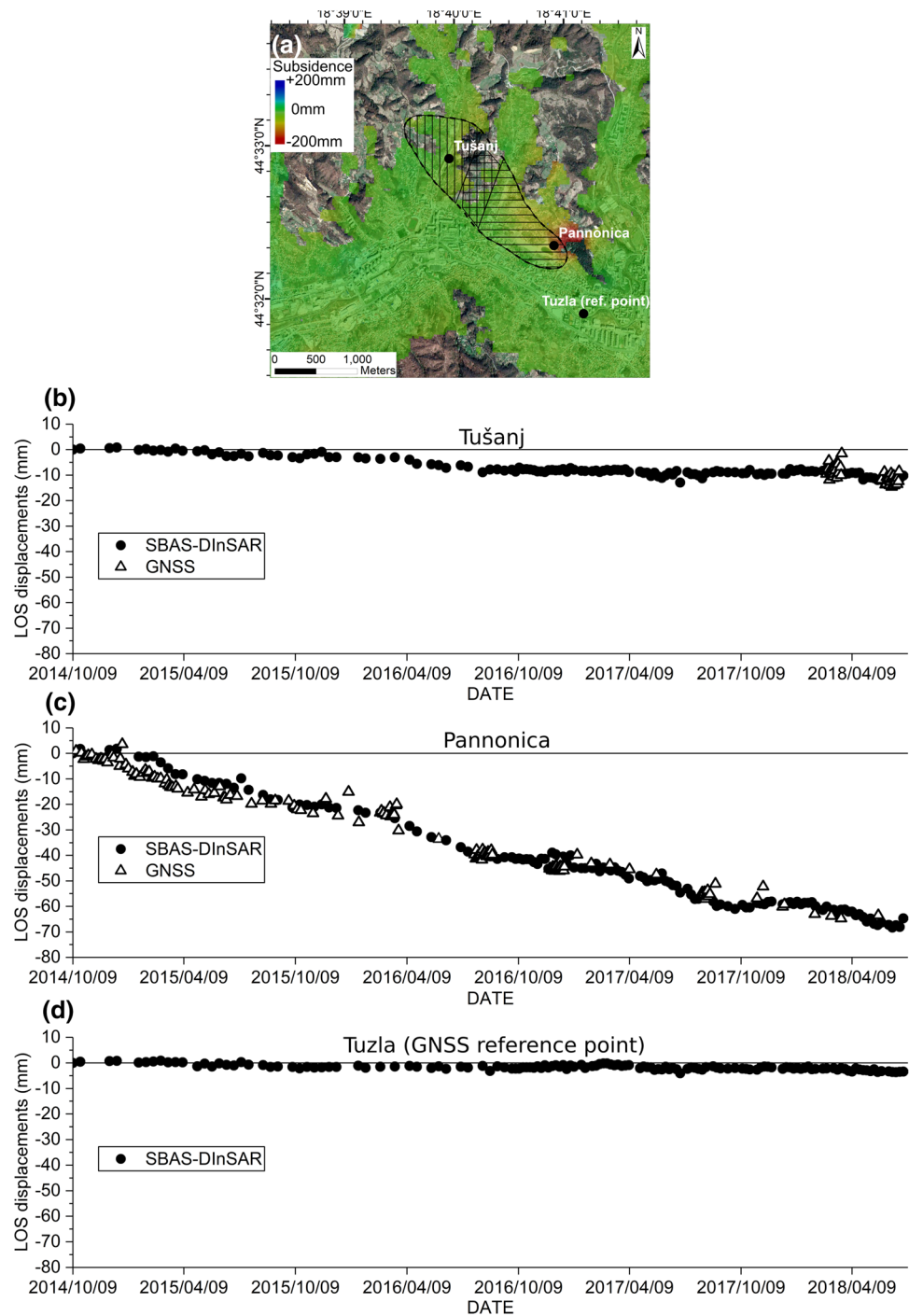
To assess the present trend of the subsidence, the time transitions from 2014 to 2019 obtained by SBAS-DInSAR are compared with the subsidence measured by GPS from 2004 to 2007 (Mancini et al. 2009a; Stecchi 2008) at the GPS measurement points, as shown in Fig. 14. Both time transitions of the subsidence by GPS and SBAS-DInSAR are presented at the selected points in Fig. 15. The average subsidence rates per year were calculated for the GPS and SBAS-DInSAR results, as shown in Table 2. The distributions of cumulative subsidence during 2014–2019 are seen to overlap in Fig. 14.

The subsidence at points 10, 11, and 14–16 reached more than several meters during 1956–2003 (see the contour lines in Fig. 14), and the average rates from 2004 to 2007 were –40 to –210 mm/year (see Table 2). SBAS-DInSAR found that the subsidence occurred at rates of –10 to –20 mm/year at points 10, 11, and 14 (solid squares in Fig. 14) and at rates of –20 to –40 mm/year at points 15 and 16 (bullets in Fig. 14) from 2014 to 2019. As shown in Fig. 15a–e, the subsidence greatly decreased from 2004 to 2019, but it is still continuing at present. Around points 15 and 16, located in the northeast portion of Pannonica Lake, the maximum subsidence occurred during 2014–2019, and its trend has been found since at least 2004 (see Fig. 3a–c).

The subsidence rates at points 5–7, 17–19, 25, 26, and 29–31 (points 5–7, 17–19, and 25 are located in Hukalo–Trnovac and points 26, 29, and 31 are located in Tušanj) decreased to –3 to –10 mm/year during the period of 2014–2019, although the rates were –3 to –200 mm/year during the period of 2004–2007. Those points are denoted by solid triangles in Fig. 14. Figure 15f–j show the time transition of subsidence at points 6, 7, 19, 25, and 26. SBAS-DInSAR found that the rate was greatly reduced at those points from 2004 to 2019, and the cumulative subsidence was smaller than that in the north and northeast portions of Pannonica Lake.

At all other points (1–4, 8, 9, 12, 20–24, 27, 33–37, and 39–44), the subsidence rates have become very small, namely, within –3 mm/year (less than –1 mm/year at most points) from 2014 to 2019, as shown in Table 2. Those points are located mainly the southwest portion of the salt deposit area (i.e., the city area) and are denoted by circles in Fig. 14. Figure 15k–p show the subsidence transition in time at points 22, 24, 36–38, and 41. During the

Fig. 11 LOS displacements obtained by SBAS-DInSAR and GNSS at GNSS stations: **a** locations of GNSS stations, **b** Pannonica station, **c** Tušanj station, and **d** Tuzla station (reference point)



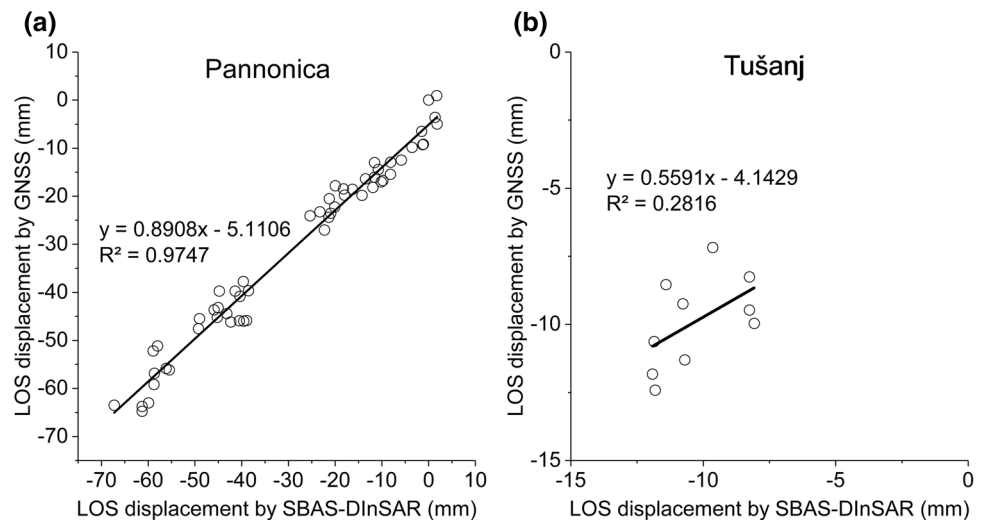
period of 2004–2007, the subsidence rates at points 22, 24, and 38 were -10 , -20 and -47 mm/year, respectively, and the rates at other points were 7 to -7 mm/year. However, during the period of 2014–2019, the rate decreased to less than -3 mm/year. SBAS-DInSAR found that the subsidence has almost vanished in this area.

There are two points (28 and 32) denoted by “X” in Fig. 14 where no results were obtained due to the low

coherence (less than the threshold value of 0.3) caused by the highly vegetated area.

From the above discussion, the subsidence in Tuzla still continues with -10 to -40 mm/year in the north and north-east portions of Pannonica Lake in spite of the termination of salt water exploitation in 2007. On the other hand, it has almost vanished in the city area. In the areas east and south of Pannonica Lake (including points 5–7 and 17–19) and

Fig. 12 Scatter plot of LOS displacements obtained by SBAS-DInSAR and GNSS at Pannonica and Tušanj stations



in the east part of Tušanj, small subsidence with a rate of up to -10 mm/year is continuing to occur. Therefore, it is important to keep monitoring the subsidence in these areas to confirm the convergence of the subsidence or to estimate the future behavior. SBAS-DInSAR can be employed as a useful and effective tool for monitoring the subsidence in Tuzla.

In this research, the LOS displacements by SBAS-DInSAR are converted to the subsidence (the vertical displacement) by using Eq. (2) under the assumption of non-horizontal displacement. A detailed discussion considering horizontal displacements together with the estimation of future behavior is needed as a future work.

6 Conclusions

This study has focused on investigating the applicability of SBAS-DInSAR for monitoring the subsidence induced by salt mining activities in Tuzla, Bosnia and Herzegovina and has compared it with the monitoring results obtained by other methodologies and in different temporal periods. The conclusions can be given as follows:

- 1 The validity and applicability of SBAS-DInSAR to monitor the subsidence induced by salt mining activities were evaluated using the former subsidence results (traditional topographic and GPS surveys) and the present real-time kinematic GNSS monitoring system. It was found that SBAS-DInSAR was able to provide the time transition of the subsidence distribution together with
- 2 The present subsidence distribution obtained by SBAS-DInSAR is much smaller than the former results obtained by the traditional topographical surveys from 1956 to 2003, and the location of the larger subsidence area was seen to have moved from the center of the salt mine deposit to the southeast border of it. The distribution shape is similar to those obtained by the former GPS survey conducted from 2004 to 2007.
- 3 SBAS-DInSAR detected that the subsidence is still ongoing in the north and northeast portions of Pannonica Lake in spite of the termination of salt water exploitation in 2007, and it has almost vanished in the city area of Tuzla. It was found that the subsidence rate was -10 to -20 mm/year and -20 to -40 mm/year in the north and northeast portions of Pannonica Lake, respectively, during the period of 2014–2019. In areas east and south of Pannonica Lake and in the east part of Tušanj, small subsidence with a rate of up to -10 mm/year is continuing to occur.
- 4 According to the above results, it is important to keep monitoring the subsidence in this area to confirm the convergence of the subsidence or to estimate the future behavior. SBAS-DInSAR can be employed as a useful and effective tool for monitoring the subsidence in Tuzla.

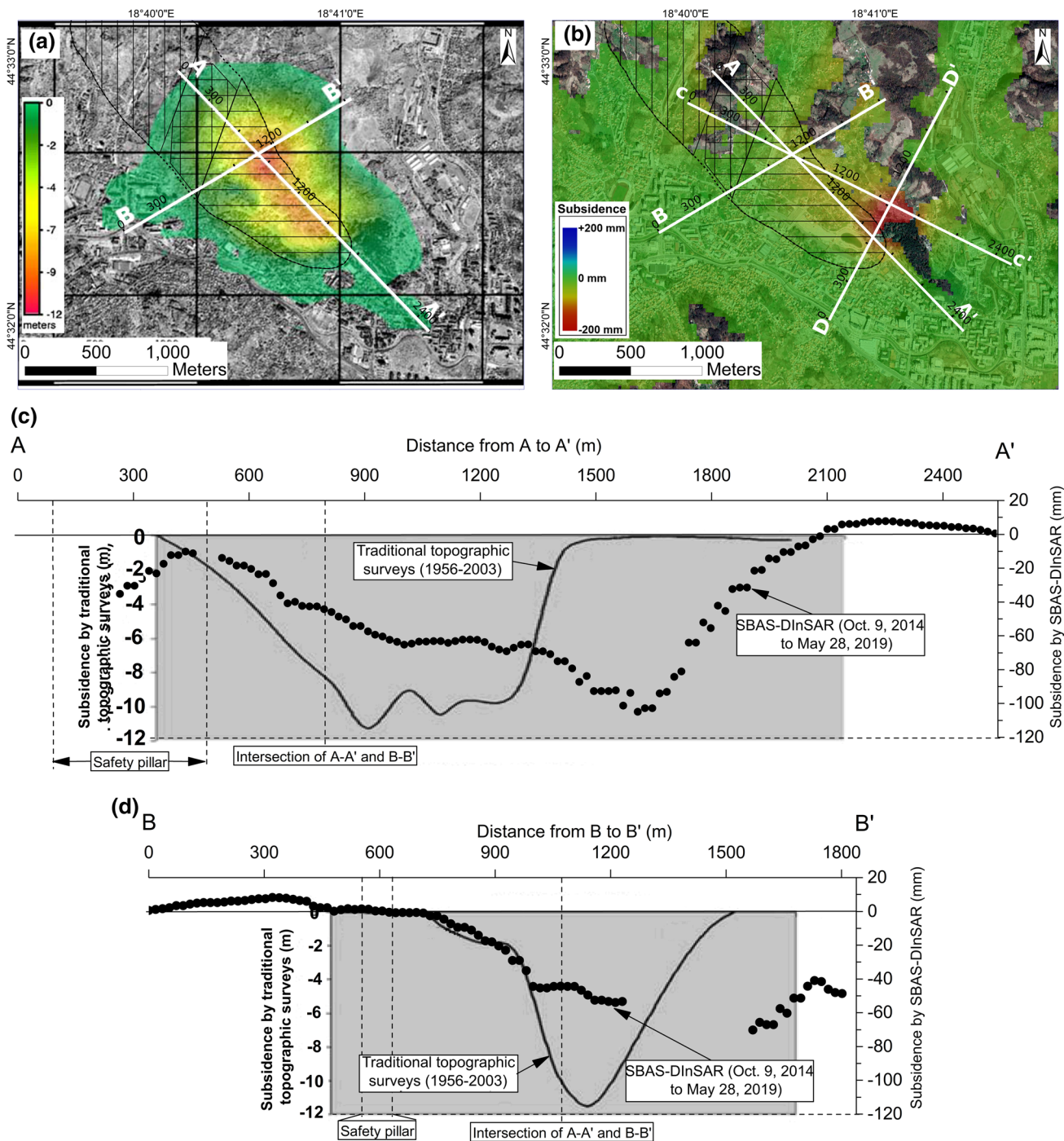


Fig. 13 Subsidence obtained by SBAS-DInSAR and traditional topographic surveys (Mancini et al. 2009b): **a** subsidence obtained by traditional topographical surveys 1956–2003 (modified from Man-

cini et al. 2009b), **b** subsidence obtained by SBAS-DInSAR October 9, 2014 to May 28, 2019, **c** section A–A', **d** section B–B', **e** section C–C', and **f** section D–D'

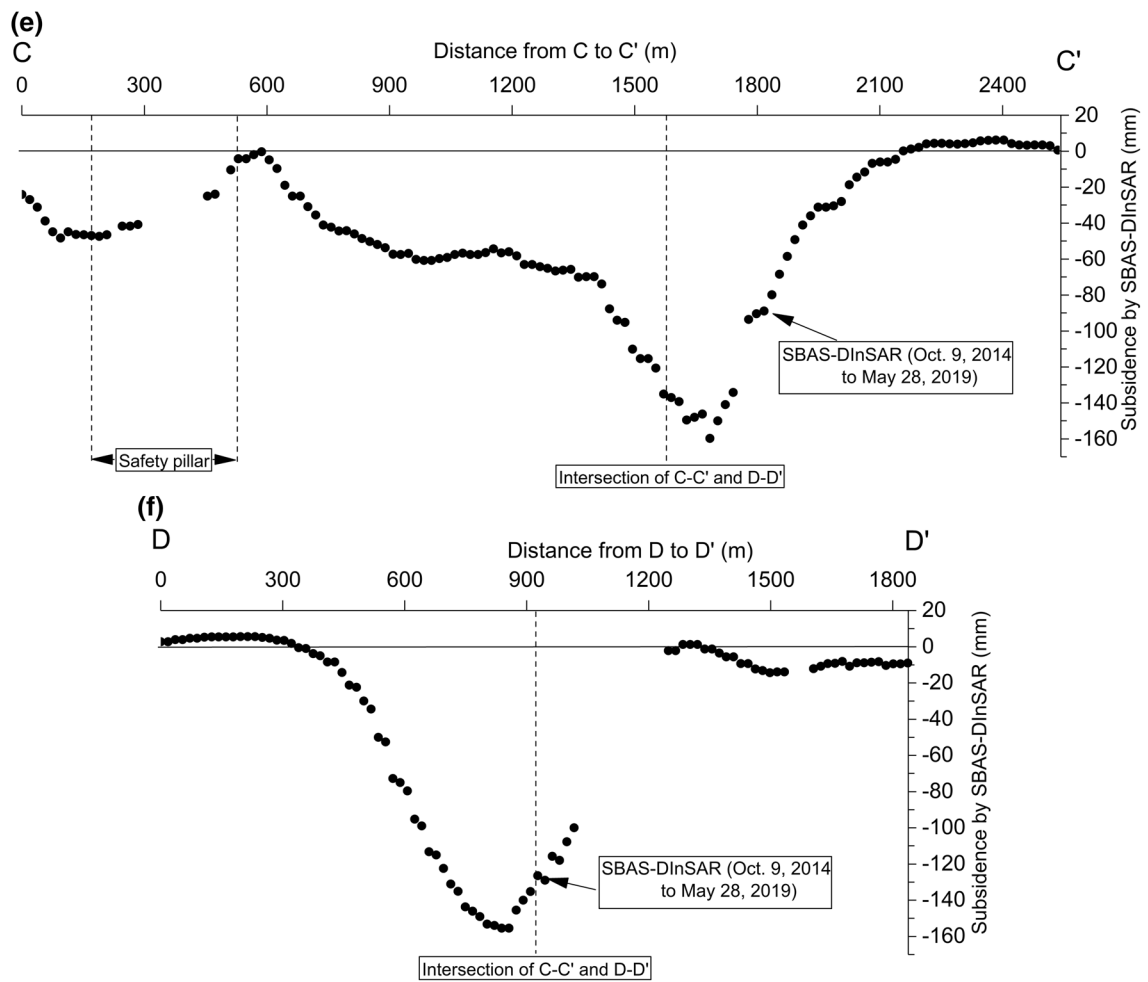
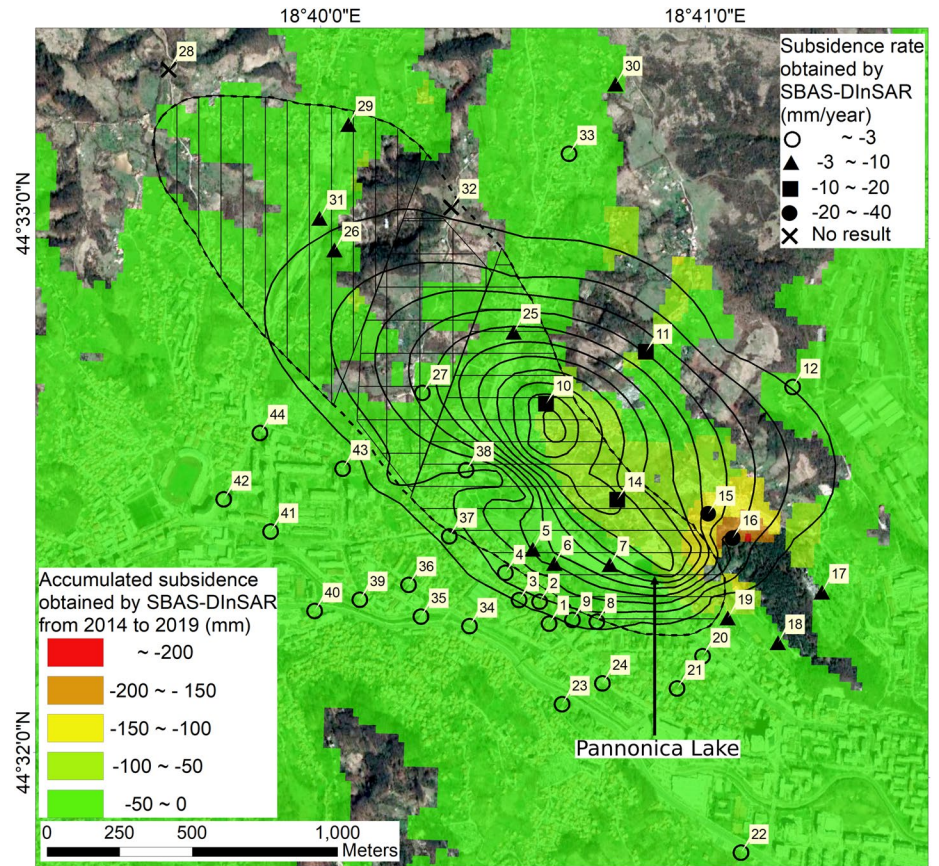


Fig. 13 (continued)

Fig. 14 Location of GPS survey points (2004–2007) superimposed with subsidence by traditional topographical surveys (contour lines, 1956–2003). The symbols of the points indicate the subsidence rate (mm/year) obtained by SBAS-DInSAR (2014–2019)



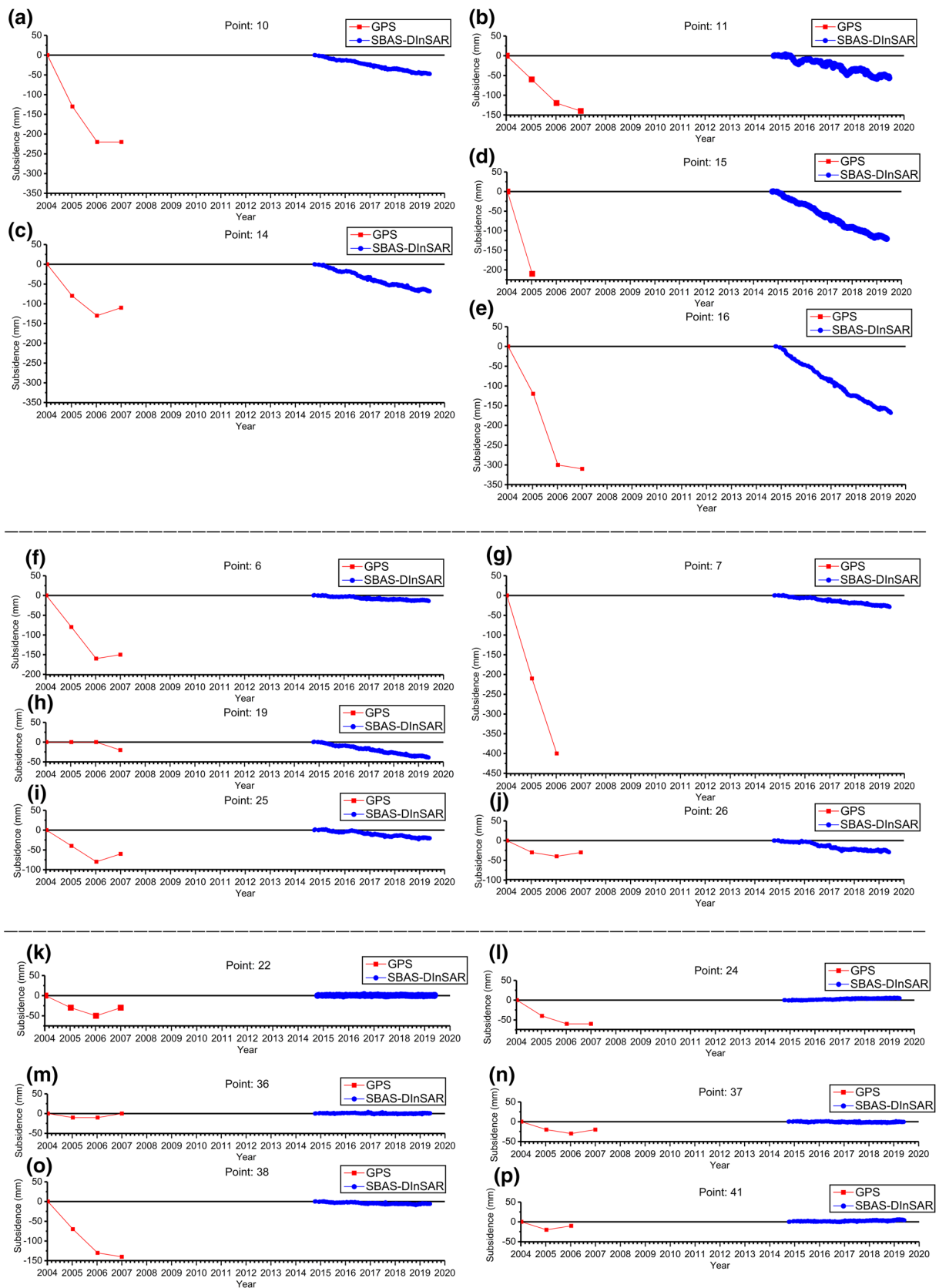


Fig. 15 Time transition of subsidence obtained by GPS surveys (2004–2007) and SBAS-DInSAR (October 9, 2014–May 28, 2019) at selected points

Table 2 Subsidence trend between two measurements periods, 2004–2007 (by GPS survey) and 2014–2019 (by SBAS-DInSAR)

Station	Average rate of subsidence (mm/year)		Symbol in Fig. 14 ^a
	2004–2007 (GPS)	2014–2019 (SBAS-DInSAR)	
1	3.33	0.89	○
2	– 6.67	0.73	○
3	0.00	0.42	○
4	– 10.00	– 0.33	○
5	– 53.33	– 3.42	▲
6	– 50.00	– 3.05	▲
7	– 200.00	– 6.21	▲
8	6.67	0.48	○
9	– 6.67	0.77	○
10	– 73.33	– 10.26	■
11	– 46.67	– 12.17	■
12	5.00	– 0.75	○
14	– 36.67	– 14.71	■
15	– 210.00	– 25.98	●
16	– 133.33	– 36.28	●
17	0.00	– 3.44	▲
18	– 6.67	– 3.33	▲
19	– 6.67	– 8.38	▲
20	0.00	– 0.77	○
21	0.00	1.04	○
22	– 10.00	0.25	○
23	– 6.67	0.56	○
24	– 20.00	1.09	○
25	– 20.00	– 4.41	▲
26	– 10.00	– 6.32	▲
27	– 3.33	– 1.71	○
28	0.00	No result	X
29	13.33	– 5.78	▲
30	– 6.67	– 5.51	▲
31	– 3.33	– 4.13	▲
32	– 10.00	No result	X
33	– 5.00	– 1.60	○
34	0.00	0.05	○
35	– 6.67	– 0.37	○
36	0.00	0.16	○
37	– 6.67	– 0.10	○
38	– 46.67	– 1.26	○
39	6.67	0.20	○
40	6.67	– 0.09	○
41	– 5.00	0.88	○
42	6.67	– 0.31	○
43	6.67	0.90	○
44	6.67	0.39	○

^a○=– 3 mm/year, ▲=– 3 to – 10 mm/year, ■=– 10 to 20 mm/year, ●=– 20 to 40 mm/year, X=No result

Acknowledgements This research was partially supported by JSPS KAKENHI (Grant-in-Aid for Scientific Research, Japan Society for the Promotion of Science) Grant no. 16H03153 and the International Collaborative Research Fund of Yamaguchi University. The SAR data were provided by the European Space Agency (ESA) and are distributed for free through the Copernicus program. The digital elevation model (DEM) and ALOS Global Digital Surface Model "ALOS World 3D-30m (AW3D30)" were provided by the Japan Aerospace Exploration Agency (JAXA). The authors wish to express their appreciation to those agencies. They also extend their appreciation to Tuzla City Municipality for their encouragement, Professor Z. Ferhatbegović for his suggestions regarding the description of geological features in Tuzla, and H. Griswold for proofreading the manuscript.

Compliance with Ethical Standards

Conflict of interest The authors wish to confirm that there are no known conflicts of interest associated with this publication and there has been no significant financial support for this work that could have influenced its outcome.

References

- Bakalović M (2005) The City on a Grain of Salt. Historical Technical Brochure. The Museum of Eastern Bosnia, Tuzla
- Barla G (2018) Numerical modeling of deep-seated landslides interacting with man-made structures. *J Rock Mech Geotech Eng* 10:1020–1036
- Berardino P, Fornaro G, Lanari R, Sansosti E (2002) A new algorithm for surface deformation monitoring based on small baseline differential SAR interferograms. *IEEE Int Geosci Rem Sens Symp* 40:2375–2383. <https://doi.org/10.1109/TGRS.2002.803792>
- Casu F, Manzo M, Lanari R (2006) Mapping ground deformation over Houston-Galveston, Texas using multi-temporal InSAR. *Rem Sens Environ* 102:195–210
- Čeliković R, Imamović E (2016) Continuous GNSS movement monitoring in the zone of influence of Tuzla salt deposit. *Int Symp Eng Geodesy* 2016:489–498
- Čeliković R, Imamović E, Salihović R, Sušić A (2014) Prostorno vremenska analiza vertikalnih pomjeranja terena u Tuzli za period 2008–2012. *Proc GEO-EXPO*. https://doi.org/10.35123/GEO-EXPO_2014_6
- Ciantia MO, Castellanza R, Fernandez-Merodo JA (2018) A 3D numerical approach to assess the temporal evolution of settlement damage to buildings on cavities subject to weathering. *Rock Mech Rock Eng* 51:2839–2862
- Cicić S (2002) Geological composition and tectonic terrain of Bosnia and Herzegovina (in Bosnian). In: Hrvatović H (ed) *Geological guidebook through Bosnia and Herzegovina*. Geological Survey of Bosnia and Herzegovina Federation, Ustanicka, pp 111–116
- Ferhatbegović Z (2004) Geological features of the central part of the Tuzla basin. In: *Dissertation, Faculty of Mining and Geology and Civil Engineering, University of Tuzla*
- Ferretti A (2014) *Satellite InSAR data: reservoir monitoring from space*. EAGE Publication, The Netherlands
- Ferretti A, Prati C, Rocca F (2000) Nonlinear subsidence rate estimation using permanent scatterers in differential SAR interferometry. *IEEE Trans Geosci Rem Sens* 38:2202–2212. <https://doi.org/10.1109/36.868878>
- Ferretti A, Monti-Guarnieri A, Prati C, Rocca F, Massonnet D (2007) *InSAR principles: guidelines for SAR Interferometry Processing And Interpretation*. ESA Publications, The Netherlands

- Herrera G, Tomas R, Vicente F, Lopez-Sanchez JM, Mallorqui JJ, Mulas J (2010) Mapping ground movements in open pit mining areas using differential SAR interferometry. *Int J Rock Mech Min Sci* 47:1114–1125
- Hrvatović H (2006) Geological guidebook through Bosnia and Herzegovina. Geological Survey of Bosnia Herzegovina Federation, Ustanicka
- Hu L, Dai K, Xing C, Li Z, Tomás R, Clark B, Shi X, Chen M, Zhang R, Qiu Q, Lu Y (2019) Land subsidence in Beijing and its relationship with geological faults revealed by Sentinel-1 InSAR observations. *Int J Appl Earth Obs Geoinf* 82:101886–101896
- Ibreljić I, Kudumović F, Ahmetbegović S (2007) Economy and ecology of natural resources in Tuzla area (Bosnia and Herzegovina) in the past and future projections. In: Proceedings of the “Joint Congress of the European Regional Science Association and ASRDLF (Association de Science Regionale de Langue Francaise), Paris, pp 1–7
- Janna C, Castelletto N, Ferronato M, Gambolati G, Teatini P (2012) A geomechanical transversely isotropic model of the Po River basin using PSInSAR derived horizontal displacement. *Int J Rock Mech Min Sci* 51:105–118
- Jokanovic B (1952) Zbornik radova, Tehnicka skola u Beogradu, pp 107–118
- Jovanovic P (1968) Contribution to the knowledge of genesis of rock salt deposits. *Tuzla Bull Geol* 13:311–317
- Jovanović O (1980) Genesis of Pretortonian Miocene sediments in North Bosnia, between Una and Orina River (in Serbian). *Geoloski Glasnik* 16:33–40
- Katzer F (1903) Historijsko rasvijanje i danasnje stanje geoloskog proucavanja Bosne i Hercegovine. *Glas.zem. muz. BiH. Sep. otis Sarajevo*
- Lanari R, Casu F, Manzo M, Zeni G, Berardino P, Manunta M, Pepe A (2007) An overview of the small baseline subset algorithm: A DInSAR technique for surface deformation analysis. *Pure Appl Geophys* 164:637–661. <https://doi.org/10.1007/s00024-007-0192-9>
- Mancini F, Stecchi F, Gabbianelli G (2009a) GIS-based assessment of risk due to salt mining activities at Tuzla (Bosnia and Herzegovina). *Eng Geol* 109:170–182. <https://doi.org/10.1016/j.enggeo.2009.06.018>
- Mancini F, Stecchi F, Zanni M, Gabbianelli G (2009b) Monitoring ground subsidence induced by salt mining in the city of Tuzla (Bosnia and Herzegovina). *Environ Geol* 58:381–389. <https://doi.org/10.1007/s00254-008-1597-1>
- Motagh M, Shamshiri R, Haghghi MH, Wetzel H-U, Akbari B, Nahavandchi H, Roessner S, Arabi S (2017) Quantifying groundwater exploitation induced subsidence in the Rafsanjan plain, southeastern Iran, using InSAR time-series and in situ measurements. *Eng Geol* 218:134–151
- Piane LD, Perello P, Baietto A, Giorza A, Musso A, Gabriele P, Baster I (2016) Mature vs. active deep-seated landslides: a comparison through two case histories in the Alps. *Rock Mech Rock Eng* 49:2189–2216
- Qu F, Lu Z, Zhang Q, Bawden GW, Kim J-W, Zhao C, Qu W (2015) Mapping ground deformation over Houston-Galveston, Texas using multi-temporal InSAR. *Rem Sens Environ* 169:290–306
- Rutqvist J, Rinaldi AP, Cappa F, Jeanne P, Mazzoldi A, Urpi L, Guglielmi Y, Vilarrasa V (2016) Fault activation and induced seismicity in geological carbon storage and lessons learned from recent modeling studies. *J Rock Mech Geotech Eng* 8:789–804
- SARMAP (2019) ENVI SARscape 5.5 Release Notes. Harris Geospatial Solution. https://www.sarmap.ch/5.5/SARscape_Release_Notes_552.pdf
- Soklić I (1959) Miocene paleogeography and origin of salt deposits in Tuzla (in Croatian). In: Hrvatović H (ed) Geological Guidebook through Bosnia and Herzegovina. Geological Survey of Bosnia and Herzegovina Federation, Ustanicka, Sarajevo, pp 117–124
- Soklić I (1964) Origin and structures of the Tuzla basin. *Geol Glasnik* 1:11–18
- Soklić I (1982) Stratigraphy and age of salt formations in Tuzla (in Croatian), Radevi AnuBiH. *Odj teh Nauka* 7:135–151
- Stecchi F (2008) Tuzla City (BiH): An example of geohazard induced by salt extraction. Dissertation, Alma, University of Bologna. <https://doi.org/10.6092/unibo/amsdottorato/1033>
- Stecchi F, Antonellini M, Gabbianelli G (2009) Curvature analysis as a tool for subsidence-related risk zones identification in the city of Tuzla (BiH). *Geomorphology* 107:316–325. <https://doi.org/10.1016/j.geomorph.2008.12.013>
- Stevanović P (1977) Geology of the Bosnia and Herzegovina, Book 3—Cenozoic periods. In: Hrvatović H (ed) Geological Guidebook through Bosnia and Herzegovina. Geological Survey of Bosnia and Herzegovina Federation, Ustanicka, pp 187–216
- Takaku J, Tadono T (2017) Quality updates of ‘AW3D’ global DSM generated from ALOS PRISM. *IEEE Int Geosci Rem Sens Symp (IGARSS)*. <https://doi.org/10.1109/IGARSS.2017.8128293>
- Tari V, Pamić J (1998) Geodynamic evolution of the northern Dinarides and the southern part of the Pannonian Basin. *Tectonophysics* 297:269–281
- Tizzani P, Berardino P, Casu F, Euillades P, Manzo M, Ricciardi GP, Zeni G, Lanari R (2007) Surface deformation of Long Valley caldera and Mono Basin, California, investigated with the SBAS-InSAR approach. *Rem Sens Environ* 108:277–289
- Tomić B, Nurić A, Nuhanović S (2005) Ground subsidence above the flooded “Tušanj” salt mine, Rudarstvo, ISSN 0353-9172 UDC 622
- Vervoort A, Declercq PY (2018) Upward surface movement above deep coal mines after closure and flooding of underground workings. *Int J Min Sci Technol* 28:53–59
- Vrabac S (1999) Facial and biostratigraphic characteristics of Badenian and Sarmatian in North Bosnia (in Bosnian), Tuzla. In: Hrvatović H (ed) Geological Guidebook through Bosnia and Herzegovina. Geological Survey of Bosnia and Herzegovina Federation, Ustanicka, pp 67–82
- Vrabac S (2005) Istorijaska geologija. University of Tuzla, pp 1–213
- Wempen JM, McCrater MK (2017) Comparison of L-band and X-band differential interferometric synthetic aperture radar for mine subsidence monitoring in central Utah. *Int J Min Sci Technol* 27:159–163
- Woo KS, Eberhardt E, Rabus B, Stead D, Vyazmensky A (2012) Integration of field characterisation, mine production and InSAR monitoring data to constrain and calibrate 3-D numerical modelling of block caving-induced subsidence. *Int J Rock Mech Min Sci* 53:166–178
- Zan FD, Guarnieri AM (2006) TOPSAR: terrain observation by progressive scans. *IEEE Trans Geosci Remote Sens* 44:2352–2360. <https://doi.org/10.1109/TGRS.2006.873853>

Publisher's Note Springer Nature remains neutral with regard to jurisdictional claims in published maps and institutional affiliations.